

Handsheets formation and mechanical testing via fiber-level simulations

Leonard H. Switzer III, Daniel J. Klingenberg, University of Wisconsin, Madison, and C. Tim Scott, USDA Forest Products Laboratory, USA

KEYWORDS: Handsheets, Networks, Simulations, Strength

SUMMARY: A fiber model and simulation method are employed to investigate the mechanical response of planar fiber networks subjected to elongational deformation. The simulated responses agree qualitatively with numerous experimental observations, suggesting that such simulation methods may be useful for probing the relationships between fiber properties and interactions and the behavior of fiber networks. Quantitative discrepancies between experiments and simulations are attributed in part to computational limitations, in addition to potential shortcomings in the underlying fiber model.

ADDRESSES OF THE AUTHORS: Leonard H. Switzer III (leonard_switzer@praxair.com), Daniel J. Klingenberg (klingen@neep.engr.wisc.edu): Department of Chemical and Biological Engineering and Rheology Research Center, University of Wisconsin, Madison, WI 53706. C. Tim Scott (cscott@facstaff.wisc.edu): USDA Forest Products Laboratory, Madison, WI 53706.

1. Introduction

Understanding the characteristics that determine the mechanical properties of fiber networks is important, for example, in controlling wet web strength and making paper with desired physical properties. Experimental investigations have demonstrated that the strength of fiber networks (e.g., wet webs, handsheets, and flocs) is influenced by a variety of fiber properties, including fiber length, coarseness (Seth 1995) aspect ratio (fiber length/diameter), flexibility (Soszynski and Kerekes 1988), and shape (Mohlin et al. 1996). Determining the relationships between network properties and fiber properties and interactions can be useful for designing and optimizing suspension compositions and processes.

Network theories have provided some insight into the factors that control the strength of fiber networks, producing relationships between fiber concentration, aspect ratio and stiffness, and the network modulus (Meyer and Wahren 1964) and yield stress (Bennington et al. 1990). Such theories, however, employ idealized models of network structure, and thus do not account for how fiber properties and interactions influence the suspension structure and the resulting impact on network properties.

Heyden and Gustafsson (2001) employed the finite element method for determining the stress-strain relationships of random fiber networks. This approach allows one to study more realistic, random networks by following the evolution of all fibers in a representative volume. Heyden and Gustafsson were able to study the effects of fiber interaction details on the failure characteristics of networks. Their method however, requires information about the initial fiber positions and orienta-

tion, and thus cannot be employed to explore how interactions influence structure formation.

Particle-level simulations offer a method for determining the structure as well as other macroscopic properties of particulate suspensions. One simply specifies the particle properties and interactions, and determines the evolution of the microstructure by numerically integrating the particles' equations of motion. An advantage of such methods is that the effects of individual particle features on macroscopic properties can be investigated systematically.

Simulations of suspensions of rigid fibers have provided relationships between the suspension structure and rheological properties and such parameters as fiber aspect ratio and concentration, in good agreement with experimental data (Yamane et al. 1994; Sundararajakumar and Koch 1997; Harlen et al. 1999). Flexible fibers have been modelled as chains of rigid bodies of various shapes linked end to end (Yamamoto and Matsuoka 1993, 1994; Ross and Klingenberg 1997). Schmid et al. (2000), Switzer (2002) and Switzer et al. (2003) modelled suspensions of flexible fibers composed of linked spherocylinders connected by ball and socket joints, with potentials in the joints to mimic the elastic resistance to bending and twisting. These simulation studies illustrated the importance of fiber equilibrium shape, flexibility, and interfiber friction in determining the structure, rheology, and flocculation behavior of fiber suspensions.

In this article, we modify the method utilized by Schmid et al. to investigate the relationships between fiber properties and interactions and the mechanical properties of planar networks. The fiber model and simulation method are briefly described in the following section. A device for experimentally probing the tensile properties of fiber handsheet samples is also briefly described. Simulated planar networks are formed by compressing a fiber suspension over a screen permeable to only the suspending fluid. The planar networks are then subjected to elongational deformation, and the required tensile force is calculated. Results of the mechanical response of planar fiber networks to elongational deformation are presented in Section 3. Numerous features of the simulated mechanical responses agree qualitatively with experimental results.

2. Methods

2.1. Fiber model and simulations

Flexible fiber suspensions are modelled as neutrally-buoyant, linked rigid bodies immersed in a Newtonian liquid. Each fiber is represented by N_{seg} rigid cylinders (length $2l$, radius b , overall fiber length $L = 2N_{\text{seg}}l$) with

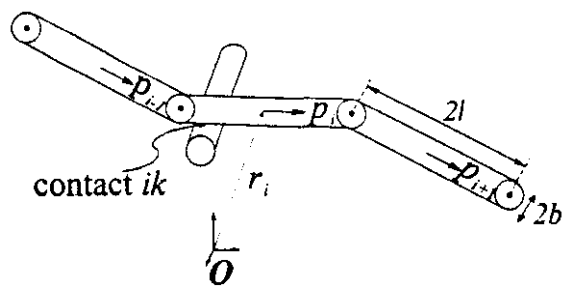


Fig 1. Schematic diagram of a model fiber composed of rigid spherocylinders linked by ball and socket joints. Here, segment i is in contact with segment k from another fiber.

hemispherical end caps, connected end-to-end by ball and socket joints (Fig 1). The motion of each fiber segment is described by Newton's equations of translational and rotational motion, in which we neglect fluid and fiber inertia. The evolution of the fiber shapes, orientations and positions are simulated by numerically integrating the equations of motion subject to the forces and torques acting on each segment. These forces and torques are described briefly below. The model and simulation method are described in more detail elsewhere (Switzer 2002).

Forces and torques acting on the fibers include: constraint forces that maintain the connectivity of the segments within each fiber: hydrodynamic forces and torques: bending and twisting potentials within the hinges to resist fiber deformation: short-range repulsive forces to prevent fiber overlap: and friction between fibers in contact. Hydrodynamic forces and torques are treated in the free-draining, zero Reynolds number limit. Bending and twisting torques are assumed to be linear in the deviations of the bending and twisting angles (θ and ϕ) from their equilibrium values (θ^{eq} and ϕ^{eq}), with bending and twisting spring constants $k_b = E_Y I / 2l$ and $k_t = E_Y J / 2l$ (E_Y is the fiber Young's modulus, and I and J are the corresponding moments of inertia). For all results reported here, $k_t = 0.67 k_b$, mimicking a linearly elastic circular cylinder with a Poisson's ratio of 0.5. Friction forces are characterized by a static coefficient of friction μ^{stat} .

Planar network formation is simulated by randomly placing fibers in a simulation cell with xy dimensions $\zeta L \times \zeta L$ ($\zeta = 2$ for all results reported here), and height $2\zeta L$ in the z -direction. A solid piston of mass M is initially located at the top ($z = 2\zeta L$), a semipermeable screen is located at the bottom ($z = 0$), and periodic boundary conditions are applied in the x and y directions. The equations of motion for the fibers and the piston are solved numerically as the falling piston forces the suspending fluid through the screen, forming a sheet-like, three-dimensional network of entangled fibers, as illustrated in Fig 2. The piston mass is chosen such that the final volume fraction of the network is $\Phi = 0.05 \pm 0.005$. For the results presented the "sheets" formed were approximately 10-15 fiber diameters in thickness, with periodic in-plane dimensions of $2L \times 2L$. We acknowledge that this method differs significantly from typical handsheet formation; it is employed here simply as a means for obtaining planar networks.

Simulation of network elongation is performed by first identifying the fiber segments that intersect the planes

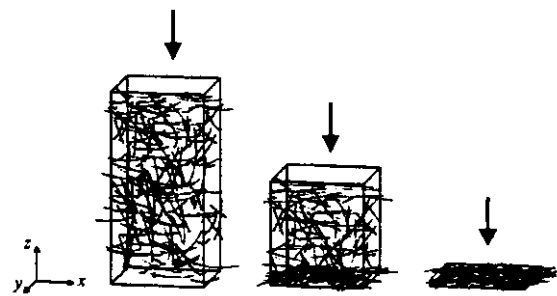


Fig 2. Illustration of sheet formation in simulations. The piston (not shown) pushes down from the top.

located at $x = \pm \zeta L / 2$ (Fig 3). The points of intersection of these segments and the planes are constrained to move at speed $\pm u_p$; the motion of the remaining segments is determined by numerical integration of their equations of motion (with the piston fixed). The tensile force T is evaluated as the sum of the forces required to displace the segments that intersect each plane at $x = \pm \zeta L / 2$, averaged over the two planes. The fiber stiffness is characterized by a dimensionless effective stiffness, $s^{eff} \equiv E_Y l / \eta_0 \dot{\gamma} L^3$, where η_0 is the suspending fluid viscosity, and $\dot{\gamma} = u_p / b$ is a characteristic deformation rate.

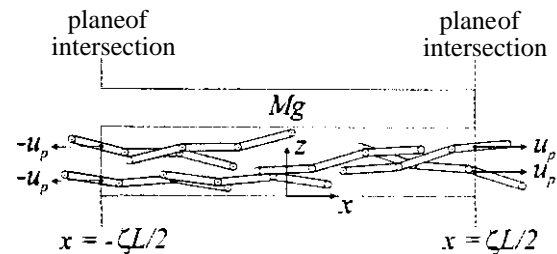


Fig 3. Schematic diagram illustrating the simulation cell after the formation of the planar network, and the planes containing the fiber segments constrained to translate in order to simulate elongation.

In the simulation of network elongation, the piston is maintained at its final position from the formation process, in contact with the network. The resulting forces on the network (in addition to interfiber friction forces) help maintain some degree of consolidation, much like surface tension on a completely saturated network. In principle, one could also model the effect of surface tension forces caused by menisci between fibers in contact to investigate effects of water content on the network behavior.

The simulation method presented here can be contrasted with that presented by Heyden and Gustafsson (2001). Their method employs a more detailed model of fiber-fiber interactions, including bonds and bond degradation, and determines the quasi-static evolution of prescribed fiber networks. As a result, their approach is well-suited for studying the mechanical response of dry sheets at small deformation rates. Our approach employs hydrodynamic forces, interfiber friction and short-range repulsion, and thus is more appropriate for studying wet web behavior at arbitrary deformation rates. We also determine the network structure by simulation, as opposed to specifying the structure a priori, and thus can explore the influence of fiber interactions on the network structure formation. We point out that both methods could in principle be modified to describe a wide range of phenomena.

2.2. Experiments

A device was constructed to measure the tensile force exerted on a fiber sheet sample and observe the network structure as it is elongated as illustrated schematically in Fig 4. The device and experimental method are summarized briefly here, and will be described in more detail in a future publication (Scott et al. 2005). The sample was held horizontally by two clamps, one attached to a 50 gram load cell, and the other attached to a screw driven at a constant speed of $2u_p \gg 8.3$ mm/min. The pulp was a nonrefined, bleached softwood market pulp screened in a Bauer-McNett fractionator. The fraction collected on the 20-mesh screen was used for this study. Handsheets of dimensions 5 cm \times 5 cm were formed in a sheet mold in which a dilute fiber suspension was drained over a 400 mesh nylon screen. The resulting networks were tested either air-dried or rewet. The sheets had a basis weight of approximately 10 g/m². The sheets were cut into strips 3.2 mm in width, with an exposed length between the clamps of 9.5 mm. Rewet samples were obtained by placing drops of water on the exposed sample edge (after cutting and placing the sample in the device) and allowing surface tension to transport the water throughout the entire network. We note that the cutting process apparently did not affect the network strength near the sample edge, as initial fiber contact failure occurred at essentially random positions across the sample width. A microscope with a CCD camera was mounted above the sample to capture images at 10 Hz as the sample was elongated.

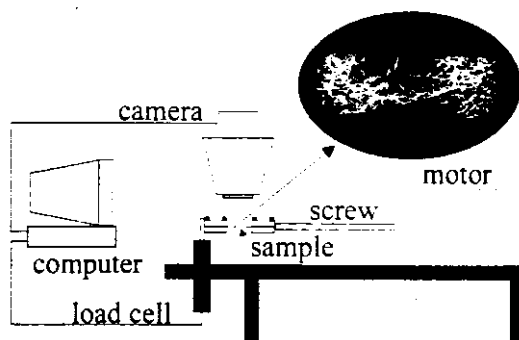


Fig 4. Schematic diagram of the apparatus developed to test small planar fiber networks.

3. Results

3.1. Experiments

As mentioned above, the assumptions employed in the simulation model make it more appropriate for examining the behavior of wet webs. For completeness, however, we will discuss experimental observations of both dry and rewet sheets.

The tensile force T is plotted as a function of engineering strain (%) for typical dry and rewet handsheet samples in Fig 5. The tensile force initially increases linearly with strain, indicative of a linear elastic response. The force then increases nonlinearly with strain, before passing through a maximum. For strains beyond the maximum, the force gradually decreases and fluctuates significantly in the dry test.

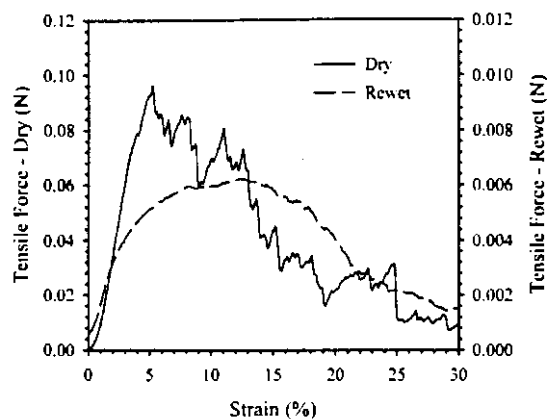


Fig 5. Tensile force as a function of strain for dry and rewet handsheets.

Images of the tension tests reveal several interesting features associated with sheet deformation. For the dry specimens, as the deformation commences, fibers start to align in the direction of extension, and some fibers bend. Within the linear region, fiber contacts appear to remain intact. However, as the maximum force is reached further deformation causes numerous contacts to break, after which fibers rapidly spring back to form a new equilibrium state. The contact breaking and reforming processes and the resulting redistribution of forces likely give rise to the dramatic tensile force fluctuations. The forces acting at new fiber contacts may include bonding and friction, but in general, fibers are not observed to rupture.

For the rewet specimens, fibers also align in the direction of sheet extension but the extent of the linear region is small. As fiber contacts break, the fibers begin to continually slip past each other. At the point of maximum force, a region of network failure becomes visible. The force then slowly diminishes to zero as fewer fibers remain in contact. Fluctuations in the tensile force are still present after the maximum, but the amplitude is smaller than that observed for the dry samples.

3.2. Simulations

Fiber network strength is influenced by a number of parameters including fiber equilibrium shape, length, flexibility, and coefficient of static friction. In all of the simulation results presented here, the fibers are composed of $N_{\text{seg}} = 5$ segments, are monodisperse with respect to length and stiffness, and interact only with short-range repulsive forces and static friction.

Fig 6 illustrates snapshots of structures from a typical simulation at three different strains $\epsilon \equiv \Delta x / \zeta L$, for a suspension of straight, flexible fibers ($S^{\text{eff}}, r_p, \theta^{\text{eq}}, \phi^{\text{eq}}, \mu^{\text{stat}} = (0.05, 75, 0, 0, 20)$). The mechanical responses for these and other conditions are described below.

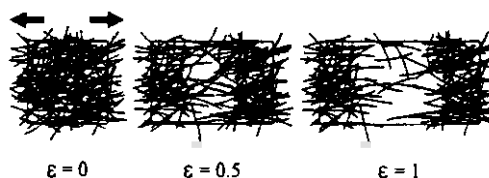


Fig 6 Snapshots of the structure of a typical simulated fiber network subjected to elongation at various deformations

3.2.1. Effects of equilibrium shape

Wood fibers display a variety of shapes, as illustrated in Fig 7(a). The equilibrium fiber shapes utilized in the simulations were either inherently straight ($\theta^{eq}=0, \phi^{eq}=0$) or U-shaped ($\phi^{eq}>0, \phi^{eq}=0$); examples are illustrated in Fig 7(b).

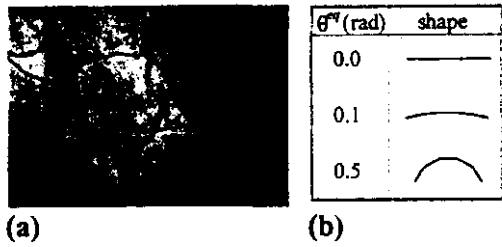


Fig 7. (a) Softwood fibers in water, and (b) examples of U-shaped fibers ($\phi^{eq}=0$) for various values of θ^{eq} .

Fiber networks were formed using straight and U-shaped fibers ($\theta^{eq} = 0.1$, and $\theta^{eq} = 0.5$), in which the remaining parameters were held constant (S^{eff}, r_p, μ^{stat}) = (0.05, 75, 20). The dimensionless tensile force $T/\eta_0 u_p L$ is plotted as a function of strain for these systems in Fig 8. Tensile force data were averaged over deformation intervals of $\Delta\epsilon \approx 0.02$. Each set of symbols in Fig 8 represents an average of two simulation runs.

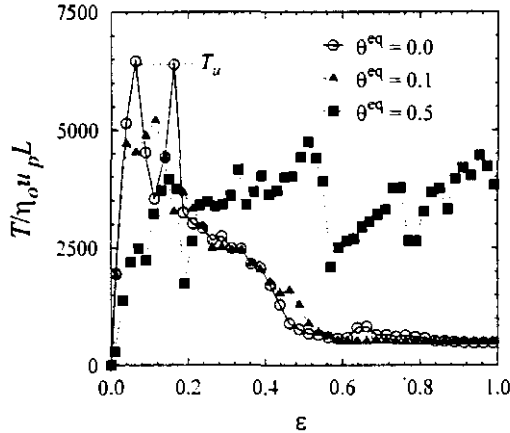


Fig 8. Dimensionless tensile force $T/\eta_0 u_p L$ as a function of strain ϵ for networks of differently shaped fibers.

Features of the response are similar to that observed experimentally for the dry and rewet samples. The tensile force initially varies linearly with deformation. The force then varies nonlinearly and passes through a maximum, accompanied with large fluctuations. The (average) rate of decrease of the tensile force after the maximum is smaller than the initial rate.

The fluctuations in tensile force correspond to fiber contacts breaking and reforming, analogous to that observed experimentally. The tensile force increases as fibers align and deform; the tensile force decreases when contacts break (i.e., when the ratio of the friction force to the repulsive force at a contact exceeds μ^{stat}). The larger rapid decreases in the tensile force correspond to multiple contacts breaking virtually simultaneously. The fact that the fluctuations are rapid implies that the fibers are relatively stiff; when a contact breaks, fibers are able to spring back and reform new contacts very quickly relative to the rate of deformation.

The straight fiber network exhibits a rapid increase in

tensile force as the sample is elongated to a maximum value defined as the network tensile strength. Networks of slightly deformed fibers ($\theta^{eq} = 0.1$) exhibit similar behavior, but with a smaller tensile strength. The tensile force for fiber networks with substantially deformed fiber ($\theta^{eq} = 0.5$) increases more slowly with increasing deformation, and does not pass through a maximum over the deformation range simulated. The different responses for networks composed of straight and highly deformed fibers correspond to different structure evolutions. As illustrated in Fig 6, networks of straight fibers develop a clear fracture zone at $\epsilon = 1.0$. In contrast, networks of highly curved fibers exhibit incomplete fracture, with the network remaining partly intact to deformations $\epsilon > 1.0$.

These simulation results are consistent with experimental observations for wet webs. The strength of wet webs tends to decrease with increasing fiber deformation (Page et al. 1985), while the stretch increases with increasing fiber deformation (Page et al. 1985; Seth 1990).

3.2.2. Effects of fiber length

Simulations were performed using fibers of various lengths (aspect ratios $r_p = 50, 75$, and 100). The fibers were U-shaped and all had the same radius of curvature $R_U = 59.5b$. The radius of curvature is defined here as the average of the radii of circles tangent to the joints and segment centers, $R_U = |1/\sin(\theta^{eq}/2) - 1/\tan(\theta^{eq}/2)|/2$. The effective stiffness $S^{eff} \equiv E_f I / \eta_0 \dot{\gamma} L^4$ was chosen to make the fiber stiffness ($E_f I$) constant [$r_p = 50 \rightarrow S^{eff} = 0.25$, $r_p = 75 \rightarrow S^{eff} = 0.05$, $r_p = 100 \rightarrow S^{eff} = 0.016$]. All fibers interacted with the same coefficient of static friction, $\mu^{stat} = 20$.

The results for the dimensionless network force $T/E_f b^2$ as a function of strain are illustrated in Fig 9. The network elastic modulus, defined as the initial slope of the tensile force as a function of strain, increases with increasing aspect ratio. The network strength increases and is shifted to larger deformations as the fiber aspect ratio is increased.

These results are consistent with experimental results reported by Seth (1995), who observed that the wet-web tensile strength of softwood pulp networks increased linearly with the average fiber length. This was attributed to longer fibers having an increased number of frictional contacts with other fibers. This is indeed observed in the simulations, where the average number of contacts per fiber (at $\phi = 0.05$) are 2.5, 2.7 and 3.2 for the systems with fiber aspect ratios 50, 75 and 100, respectively.

3.2.3. Effects of flexibility and friction

Fiber networks with various values of the effective stiffness S^{eff} were simulated with $(r_p, \theta^{eq}, \phi^{eq}, \mu^{stat}) = (75, 0.1, 0, 20)$. Fig 10 illustrates the results for the dimensionless tensile force $T/\eta_0 u_p L$ as a function of strain for $S^{eff} = 0.005, 0.025, 0.05$ and 0.5 . As S^{eff} increases, the tensile strength and the elastic modulus of the network increase. This is not unexpected as the force required to deform individual fibers increases with increasing fiber stiffness. The network strength increases more slowly as S^{eff} is increased beyond 0.05.

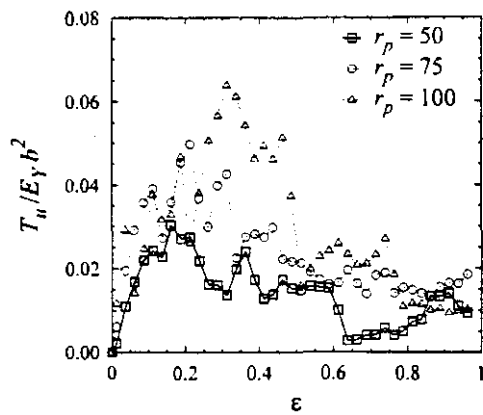


Fig 9. Dimensionless tensile force $T/E_p b^2$ as a function of Strain ϵ for fibers of different aspect ratios.

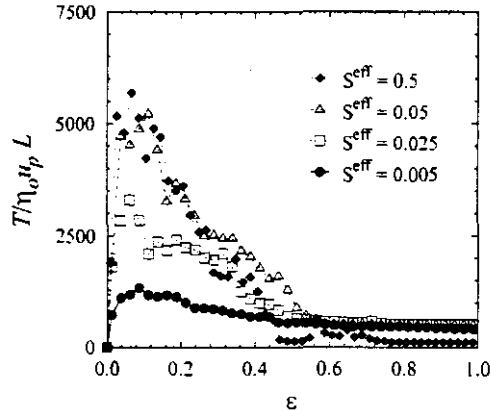


Fig. 10. Dimensionless tensile force $T/\eta_0 U_p L$ as a function of strain ϵ for planar fiber networks at various effective stiffness values.

Elongation of fiber networks with $(r_p, S^{\text{eff}}, \theta^{\text{eq}}, \phi^{\text{eq}}) = (75, 0.05, 0.1, 0)$ were simulated for various values of μ^{stat} , and the results for the dimensionless tensile force as a function of deformation are presented in Fig 11. As expected the network strength increases with increasing μ^{stat} . The elastic modulus of the network also increases with μ^{stat} .

Soszynski and Kerekes (1988) proposed that the cohesive forces that hold fibers within networks are caused by inter-fiber friction. The strength of the friction force is proportional to the normal force between contacting fibers, and this normal force is a function of the fiber stiffness. The simulation results are thus consistent with the notion that fiber flexibility and friction contribute to the overall strength of a fiber network.

4. Discussion

The simulations qualitatively reproduce numerous experimentally observed features of the mechanical response of planar fiber networks. However, as described below, quantitative agreement is lacking. This discrepancy is due at least in part to computational limitations that prevent us from performing the simulations for actual experimental conditions, in addition to possible shortcomings of the model.

The values of μ^{stat} employed in the simulations are much larger than those measured experimentally [$\mu^{\text{stat}} \approx 0.5$ for contacting cellulose surfaces and cellulose fibers (Zauscher and Klingenberg 2001, Shchukin et al. 1998)]. For $\mu^{\text{stat}} \leq 1$, the simulated networks exhibit no significant tensile strength beyond that produced by hydrodynamic

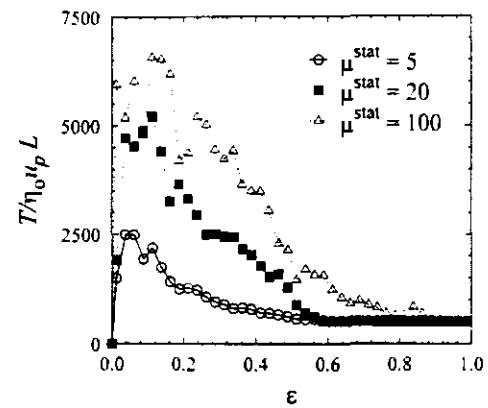


Fig. 11. Dimensionless tensile force $T/\eta_0 U_p L$ as a function of strain ϵ for planar fiber networks in which the coefficient of friction is varied. drag. Possible reasons that such large values of μ^{stat} are needed to produce mechanical responses similar to those observed experimentally are related to the nature of contacts formed and the values of S^{eff} employed in the simulations.

Wood fibers can bond, and large coefficients of friction may serve to approximately model fiber bonding. Explicitly adding fiber bonding to the present model should produce similar mechanical responses at lower values of μ^{stat} (i.e., interfiber bonds increase the load at contact points, thus increasing the friction force at fixed μ^{stat}). Wood fibers are also significantly more complex than the simple fiber model employed here. Fibrillation and other surface features may impede fibers from sliding over one another, yielding larger apparent coefficients of friction. Seth (1995) observed that the tensile strength of wet softwood fiber webs decreased with fiber coarseness. Fiber coarseness is approximately proportional to wall thickness, and thus fibers that are less coarse can more easily collapse to ribbon-like structures, producing greater contact areas. Such features are not included in the present model. Finally, surface tension forces arising from water menisci between fibers in contact act to increase the normal force between fibers, thus increasing the lateral friction forces. Thus including such surface tension forces should produce similar behavior with smaller coefficients of friction.

The values of the effective stiffness $S^{\text{eff}} \equiv E_f I / \eta \dot{\gamma} L^4$ used in the simulations are also significantly smaller than those encountered experimentally. Choosing parameter values representative of the experimental systems described in Section 2.2 [$E_f I = 10^{-12} \text{ Nm}^2$ (Tam Doo and Kerekes 1981), $\eta_0 = 2 \times 10^{-5} \text{ Pa}\cdot\text{s}$ for air and $\eta_0 = 1 \times 10^{-3} \text{ Pa}\cdot\text{s}$ for water (Bird et al. 2002), $u_p = 1.9 \text{ mm/min}$, $b = 16 \mu\text{m}$, $\dot{\gamma} = u_p/b = 2.0 \text{ s}^{-1}$, and $L = 2.5 \text{ mm}$], the experimental values of the dimensionless stiffness are $(S^{\text{eff}})_{\text{exp}} \approx 640$ for the dry samples and $(S^{\text{eff}})_{\text{exp}} \approx 13$ for the rewet samples, much larger than those employed in the simulations ($S^{\text{eff}} \leq 0.5$). Computational limitations prevent us from performing simulations with such large stiffnesses. As the stiffness increases, the maximum allowable time step for stable integration of the equations of motion decreases rapidly. Thus simulations for $S^{\text{eff}} > 0.5$ cannot be performed in a reasonable time.

Switzer (2002) performed simulations similar to that employed here to study the flocculation behavior of flexible fiber suspensions. Flocculation was observed for

various combinations of S^{eff} and μ^{stat} . As S^{eff} was increased, the mechanical integrity of model fiber flocs was maintained for smaller values μ^{stat} . This suggests that qualitative agreement between experimental measurements and simulations of the mechanical response of planar fiber networks may be achieved for reasonable values of the coefficient of friction if simulations could be performed for larger values of S^{eff} .

Finally, we consider the magnitudes of the tensile forces. The experiments produced tensile forces of magnitude $T \approx 0.1$ N for dry samples and $T \approx 6 \times 10^{-3}$ N for rewet samples (see Fig 5). The maximum dimensionless tensile forces produced by the simulations are of magnitude $T/\eta_0 u_p L \approx 5 \times 10^{-3}$, obtained for $S^{\text{eff}} \geq 0.05$ (Fig 10). Choosing the parameter values employed above, along with $\eta_0 = 0.26$ Pa-s (to match the simulated value of $S^{\text{eff}} = 0.05$), the dimensional simulated tensile forces are of magnitude $T \approx 1 \times 10^{-4}$ N, significantly smaller than the experimentally measured values.

The difference between the measured and simulated tensile forces may be due to shortcomings in the model (e.g., neglecting the effects of surface tension in wet films), or from the computational limitations that prevent us from simulating the precise experimental conditions. Resolving these issues will require either overcoming the computational limitations, conducting experiments under conditions that can be simulated efficiently, or including more realistic models of forces acting between fibers.

5. Conclusion

We have presented a model and simulation method to investigate the mechanical response of planar, 3D networks of entangled fibers subjected to elongational deformation. Simulated mechanical responses contain features similar to that measured experimentally. The trends observed as the fiber shape and length are varied agree with experimentally observed trends. The dependence of the mechanical response on the coefficient of friction and fiber stiffness are consistent with the elastic interlocking mechanism of network strength proposed previously. Thus it appears that such simulation methods may be useful for probing the effects of fiber features and interactions on the mechanical properties of fiber networks.

Quantitative agreement with experiments, however, is lacking. The discrepancies may be attributed to shortcomings of the model, as well as computational limitations that prevent us from simulating precisely the conditions employed in typical experiments. There are several obvious differences between the simplified fiber model employed here and actual fibers used in experiments; real paper contains a non-uniform distribution of fibers of varying length, shape, flexibility, and surface features. Accurately modeling these features is computationally challenging. In this paper, we have demonstrated the utility of the model for systematically probing the effects of individual fiber features and interactions on network properties that would otherwise be very difficult to measure experimentally. Resolving the

discrepancies requires either overcoming the computational limitations or conducting experiments under conditions more amenable to the simulations.

Acknowledgments

This research was supported in part by the USDA NRI Competitive Grants Program (award no. 2001-35103-09933).

Literature

- Bennington, C. P. J., Kerekes, R. J. and Grace, J. R.** (1990): The yield stress of fibre suspensions, *Can. J. Chem. Eng.* 68, 748.
- Bird, R. B., Stewart W. E. and Lightfoot, E. N.** (2002): "Transport Phenomena", Wiley, New York 2nd ed.
- Harlen, O. G., Sundararajakumar, R. R. and Koch, D. L.** (1999): Numerical simulations of a sphere settling through a suspension of neutrally buoyant fibres, *J. Fluid Mech.* 388, 355.
- Heyden, S. and Gustafsson, P. J.** (2001): Stress-strain performance of paper and fluff by network modeling, in "The Science of Papermaking", Trans. 12th Fundamental Res. Symp. in Oxford, C. F. Baker (ed.), The Pulp Paper Fundamental Res. Soc., 2001, p. 1385.
- Meyer, R. and Wahren, O.** (1964): On the elastic properties of three-dimensional fibre networks, *Svensk. Papperstidn.*, 67(10), 432.
- Mohlin, U., Dahlbom, J. and Hornatowska, J.** (1996): Fiber deformation and sheet strength, *Tappi J.* 79(6), 105.
- Page, D. H., Seth, R. S., Jordan, B. D., and Barbe, M. C.** (1985): Curl, crimps, kinks and microcompressions in pulp fibers—their origin, measurement and significance. in *Papermaking Raw Materials*, Transactions of the 8th Fundamental Research Symposium, Mechanical Engineering Publications, London, 183.
- Ross, R. F. and Klingenberg, D. J.** (1997): Dynamic simulation of flexible fibers composed of linked rigid bodies. *J. Chem. Phys.* 106, 2949.
- Schmid, C. F., Switzer, L. H. and Klingenberg, D. J.** (2000): Simulations of fiber flocculation: effects of fiber properties and interfiber friction, *J. Rheol.* 44, 781.
- Scott, C. T., Switzer III, L. H. and Klingenberg, D. J.** (2005): Network rupture in small, planar fiber networks", to be published.
- Seth, R. S.** (1990): Fibre quality factors in papermaking—II. The importance of fibre coarseness, *MRS Symposium Proceedings*, 197, 143.
- Seth, R. S.** (1995): The effect of fiber length and coarseness on the tensile strength of wet webs: a statistical geometry explanation, *Tappi J.* 78(3):99.
- Shchukin, E. D., Videnskii, I. V., Amelina, E. A., Bessonov, A. I., Parfenova, M., Aranovich, G., and Donokhi, M.** (1998): Adhesion of cellulose fibers in liquid media: 2. Measurement of contact force of attraction, *Colloid J.* 60(5), 541.
- Soszynski, R. M. and Kerekes, R. J.** (1988): Elastic interlocking of nylon fibers suspended in liquid. Part 1. Nature of cohesion among fibers. *Nordic Pulp Pap Res. J.* 4, 172.
- Sundararajakumar, R. R. and Koch, D. L.** (1997): Structure and properties of sheared fiber suspensions with mechanical contacts, *J. Non-Newt. Fluid Mech.* 73, 205.
- Switzer III, L. H.** (2002): "Simulations of Systems of Flexible Fibers", PhD thesis, University of Wisconsin-Madison,
- Switzer, L. H., Scott, C. T. and Klingenberg, D. J.** (2003): Simulations of fiber floc dispersion in linear flow fields, *Nordic Pulp Paper Res. J.* 18(2), 141.
- Tam Doo, PA. and Kerekes, R. J.** (1981): A method to measure wet fiber flexibility, *Tappi* 64(3), 113.
- Yamamoto, S. and Matsuoka, T.** (1993): A method for dynamic Simulation of rigid and flexible fibers in a flow field, *J. Chem. Phys.* 98, 644.
- Yamamoto, S. and Matsuoka, T.** (1994): Viscosity of dilute suspensions of rodlike particles: a numerical simulation method, *J. Chem Phys.* 100, 3317.
- Yamane, Y., Kaneda, Y. and Doi, M.** (1994) Numerical simulation of semi-dilute Suspensions of rodlike particles in shear flow, *J. Non-Newt. Fluid Mech.* 54, 405.
- Zauscher, S. and Klingenberg, D. J.** (2001): Friction between cellulose surfaces measured with colloidal probe microscopy. *Coll. Surf. A* 178, 213.

Manuscript received October 31, 2003

Accepted June, 2004

Switzer III, Leonard H.; Klingenberg, Daniel J.; Scott, C. Tim, 2004. Handsheet formation and mechanical testing via fib
level simulations. Nordic Pulp and Paper Research Journal. 19(4): 434-439.